Supporting Information

Construction of 3D Si@Ti@TiN Thin Film Arrays for Aqueous Symmetric Supercapacitors

Binbin Wei,[a] Hanfeng Liang,[a,*] Zhengbing Qi,[b] Dongfang Zhang,[a] Hao Shen,[a] Wenshen Hu,[a] and Zhoucheng Wang[a,*]

[a] College of Chemistry and Chemical Engineering, Xiamen University, Xiamen 361005, People's Republic of China

[b] Key Laboratory of Functional Materials and Applications of Fujian Province, School of Materials Science and Engineering, Xiamen University of Technology, Xiamen 361024, People's Republic of China

*Email: hfliang@xmu.edu.cn; zcwang@xmu.edu.cn

Experimental Details

Fabrication of Si arrays

Single polished silicon (100) wafers were immersed into a mixed solution of concentrated sulfuric acid and hydrogen peroxide with a volume ratio of 3:1, which was then heated at 235 °C for 15 min. Afterwards, the silicon wafers were carefully washed and rinsed several times using distilled water. After being dried at 135 °C for 12 h in a drying oven, photolithographic technique was used to produce a series of circular shaped photoresist dots on the silicon wafer substrates using photoetching machine (MA6). Finally, the silicon wafers went through a deep silicon etching process to obtain the Si arrays.

Fabrication of Si@Ti@TiN thin film arrays

In order to prepare the Si@Ti@TiN thin film arrays, Ti/TiN thin films were deposited onto Si arrays by reactive magnetron sputtering technology using a Ti target (Φ76 × 5 mm, 99.995% purity) in a sputtering machine that was degassed by a mechanical pump and a molecular pump to reach the base pressure of 6×10^{-4} Pa as demonstrated in our previous case.[1] During sputtering process, the total gas flow was kept constant at 60 sccm and the DC power applied to Ti target was fixed at 250 W. Firstly, pure Ti thin films were deposited under Ar atmosphere at a pressure of 0.6 Pa for 5, 10 and 15 min. Then, TiN thin films were deposited under 2.0 Pa of pressure with the inlet of Ar and N_2 (9 vol.%) for 30 min. For comparison, TiN and Ti/TiN thin films were also directly deposited onto the untreated silicon (100) wafers under the same conditions by reactive magnetron sputtering technology.

Material characterization

Scanning electron microscopy (SEM, ZEISS Sigma) operated at 20 kV was employed to observe the morphologies of the samples. The crystal structure identification was characterized by X-ray diffraction (XRD, Philips X'pert PRO) with Cu K_α radiation. Raman spectroscopy was recorded on an XploRA Raman using 532 nm excitation source. X-ray photoelectron spectroscopy (XPS) was done on a PHI-Quantum 2000 instrument to investigate the surface compositions using Al K_α radiation.

Electrochemical performance tests

The electrochemical behaviours of the samples were evaluated by cyclic voltammetry (CV), galvanostatic charge-discharge (GCD), and electrochemical impedance spectroscopy (EIS) on a CHI 660E electrochemical workstation. 0.5 M H_2SO_4 aqueous solution was used as the electrolyte. The electrochemical measurements of single electrodes were carried out in a three-electrode setup using the samples as the working electrode (exposed area 1 × 1 cm^2, mass loading ~ 0.39 mg cm^{-2}), an Ag/AgCl and a Pt wire as the reference and counter electrodes, respectively. To assemble the symmetric supercapacitor devices, two identical Si@Ti@TiN thin film arrays were used as the

positive and negative electrodes, which were clamped together and isolated by a Celgard 3501 separator.

Calculations

The areal specific capacitance (C_a, mF cm^{-2}) of single electrodes was obtained from GCD method based on the following equation:

$$C_a = I\Delta t/(s\times\Delta U) \quad (1)$$

Whereas for the symmetric supercapacitor devices, the cell capacitance (C_{cell}, mF cm^{-3}) was calculated according to the following equation (based on GCD data):

$$C_{cell} = I\Delta t/(V\times\Delta U) \quad (2)$$

The energy density (E, mWh cm^{-3}) and power density (P, W cm^{-3}) of the symmetric supercapacitor devices were estimated through the equations below:

$$E = C_{cell}\times\Delta U^2/(2\times 3.6) \quad (3)$$

$$P = 3.6E/\Delta t \quad (4)$$

where I (mA) is the constant discharging current, Δt (s) the discharge time, s (cm^2) the surface area of single electrodes, V (cm^3) the total volume of the whole supercapacitor device, and ΔU (V) the potential window.

Additional Figures and Data

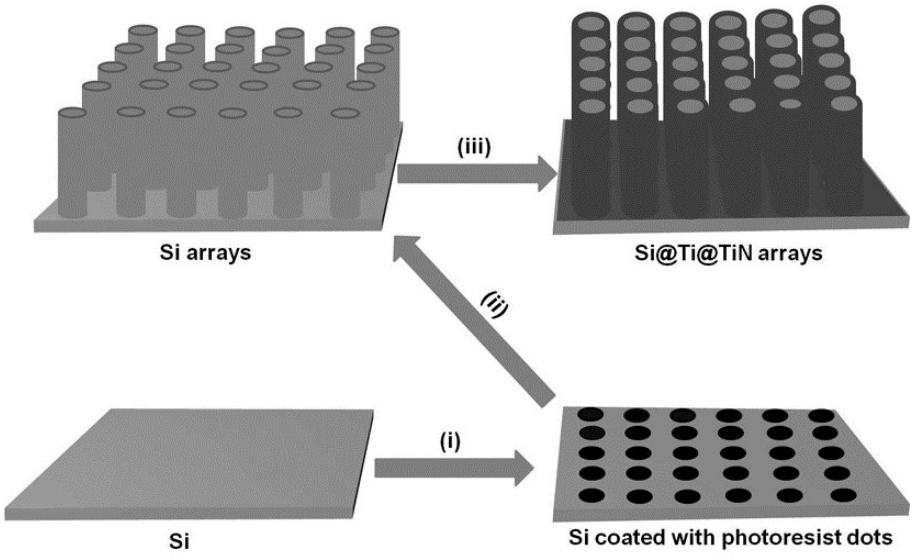

Fig. S1 Schematic illustration for the design of Si@Ti@TiN thin film arrays: (i) Photolithographic technique, (ii) Deep silicon etching procedure, (iii) Magnetron sputtering method.

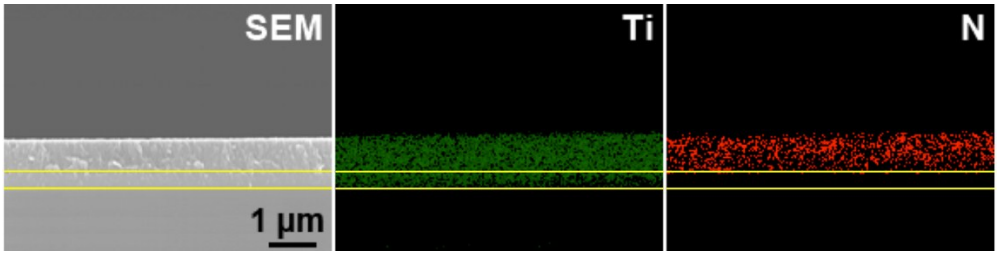

Fig. S2 SEM image of Ti/TiN thin films and EDX mapping images of Ti and N elements.

In order to verify the composition of the red-lined region (Fig. 1e), we have performed the EDX mapping characterization. The result reveals a thin, well-defined Ti transition layer as indicated by the yellow lines.

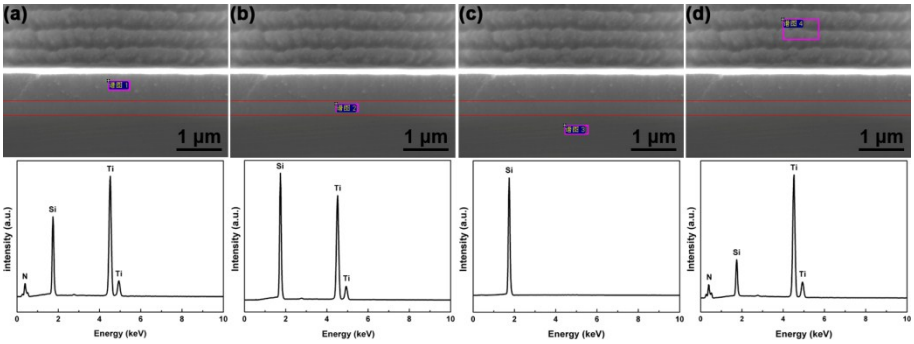

Fig. S3 SEM images and the corresponding EDX spectra of Si@Ti@TiN thin film arrays.

Three layers can be clearly identified, namely TiN, Ti, and Si from top to bottom, confirming the formation of Si@Ti@TiN thin film arrays.

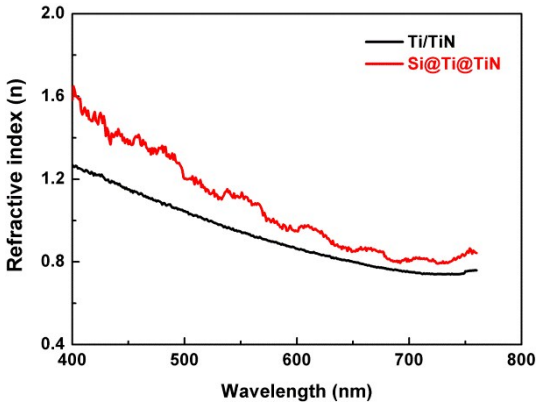

Fig. S4 Refractive index versus wavelength for Ti/TiN and Si@Ti@TiN thin films.

We have performed the ellipsometry measurements, a technique that has been widely used to determine the porosity of thin film materials. As shown in Fig. S4, the refractive index of Si@Ti@TiN (n_1) is obviously larger than that of Ti@TiN (n_2) in the visible range, which suggests a higher void content and internal surface area for the former.

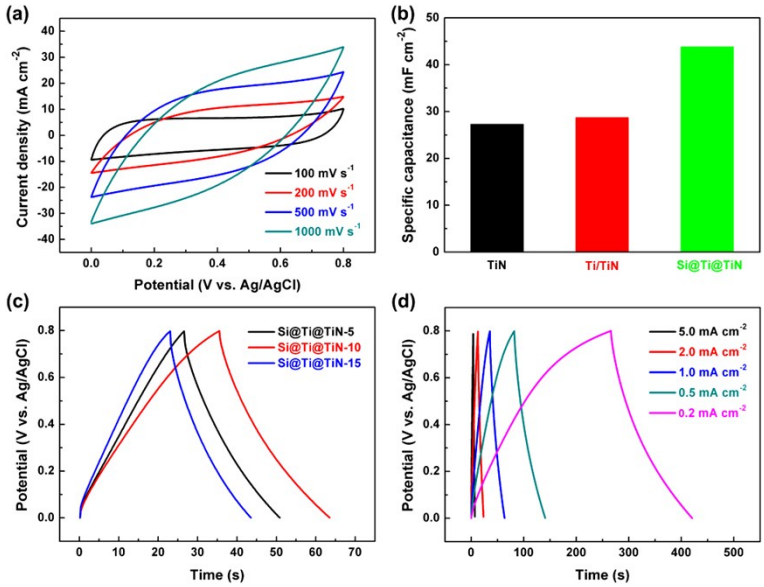

Fig. S5 (a) CV curves collected at different scan rates of Si@Ti@TiN thin film array electrodes. (b) Comparison of specific capacitance values at 1.0 mA cm^{-2} for TiN thin film, Ti/TiN thin film and Si@Ti@TiN thin film array electrodes. (c) Comparison of GCD curves at a current density of 1.0 mA cm^{-2} for Si@Ti@TiN thin film array electrodes with different Ti interlayer deposition times. (d) GCD curves measured at different current densities of Si@Ti@TiN thin film array electrodes.

In order to study the effect of Ti interlayer on the electrochemical performance, a series of control experiments based on different deposition times (5, 10 and 15 min) were carried out. According to different Ti interlayer deposition times, Si@Ti@TiN thin film arrays were labeled as Si@Ti@TiN-5, Si@Ti@TiN-10 and Si@Ti@TiN-15, respectively.

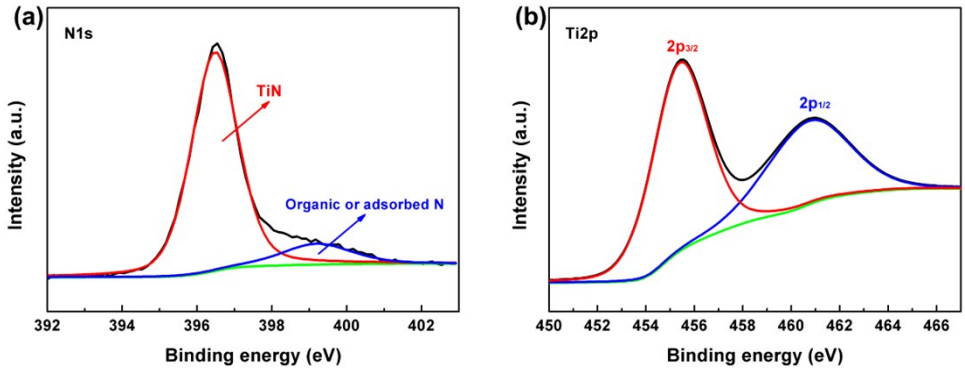

Fig. S6 XPS spectra of Si@Ti@TiN thin film array electrodes after 20000 cycles: (a) N 1s and (b) Ti 2p.

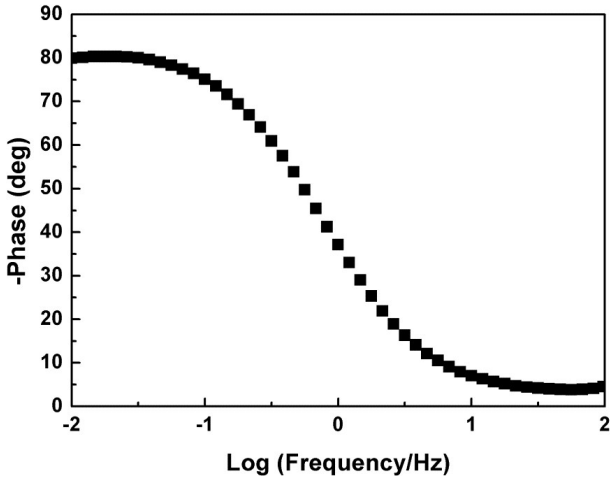

Fig. S7 Bode phase angle plot of Si@Ti@TiN thin film array electrodes.

Table S1 The electrochemical performances of recently reported metal nitrides for supercapacitors

Nitrides	Specific capacitance	Cycling performance	Reference
Si@Ti@TiN thin film array	43.8 mF cm^{-2} at 1.0 mA cm^{-2} 139.1 mF cm^{-2} at 100 mV s^{-1}	99.5% after 20000 cycles	This work
CrN thin film	12.8 mF cm^{-2} at 1.0 mA cm^{-2}	92.1% after 20000 cycles	[2]
Porous CrN thin film	31.3 mF cm^{-2} at 1.0 mA cm^{-2}	94% after 20000 cycles	[3]
TiN thin film	8.8 mF cm^{-2} at 100 mV s^{-1}		[4]
VN thin film	22.8 mF cm^{-2} at 100 mV s^{-1}	67.2% after 1000 cycles	[5]
TiVN thin film	5.6 mF cm^{-2} at 100 mV s^{-1}	99% after 10000 cycles	[6]
RuN thin film	6 mF cm^{-2} at 200 mV s^{-1}		[7]
TiN/CNT	25.5 mF cm^{-2} at 100 mV s^{-1}	90.9% after 20000 cycles	[8]
G/TiN NTA	25.2 mF cm^{-2} at 100 mV s^{-1}	86.1% after 1000 cycles	[9]
TiN@C nanotube	19.4 mF cm^{-2} at 10 mV s^{-1}	80% after 10000 cycles	[10]
γ-Mo_2N thin film	52.4 mF cm^{-2} at 10 mV s^{-1}	102% after 2000 cycles	[11]
Nitrided Titanium	0.037 mF cm^{-2} at 50 mV s^{-1}		[12]
VN power	5.4 mF cm^{-2} at 100 mV s^{-1}	64.8% after 400 cycles	[13]
Mesoporous NbN	37.0 mF cm^{-2} at 0.2 mA cm^{-2}	80% after 1000 cycles	[14]
Mesoporous GaN	24.17 mF cm^{-2} at 0.5 mA cm^{-2}	96% after 50000 cycles	[15]

Table S2 Cell capacitance, energy density, and power density of the symmetric supercapacitor devices at different current densities

Current density (mA cm^{-2})	0.2	0.5	1.0	2.0
Volumetric capacitance (F cm^{-3})	230.9	201.3	185.2	153.0
Specific energy density (mWh cm^{-3})	20.5	17.9	16.5	13.6
Specific power density (W cm^{-3})	0.86	2.1	4.3	8.6

Table S3 Comparison of the performance of the current device and other related devices in the literature

Electrode materials	**Energy density (mWh cm^{-3})**	**Power density (W cm^{-3})**	**Reference**
Si@Ti@TiN thin film array	20.5	0.86	This work
TiN thin film	17.6	1.1	[1]
CrN thin film	8.2	0.7	[2]
Porous CrN thin film	14.4	0.3	[3]
TiN nanowire	0.06	0.12	[16]
2D MoN	0.0083	0.13	[17]
Corn-like TiN	2	4	[18]
TiN nanoarray	0.25	0.2	[19]
TiN-Fe_2N ASC	0.05	0.61	[20]
VN nanowire	0.09	0.26	[21]
VN/CNT hybrid electrode	0.54	0.4	[22]

References Cited in Supporting Information

1 B. B. Wei, H. F. Liang, D. F. Zhang, Z. B. Qi, H. Shen and Z. C. Wang, *Mater. Renew. Sustain. Energy*, 2018, **7**, 11.

2 B. B. Wei, H. F. Liang, D. F. Zhang, Z. T. Wu, Z. B. Qi and Z. C. Wang, *J. Mater. Chem. A*, 2017, **6**, 2844-2851.

3 B. B. Wei, G. Mei, H. F. Liang, Z. B. Qi, D. F. Zhang, H. Shen and Z. C. Wang, *J. Power Sources*, 2018, **385**, 39-44.

4 A. Achour, R. L. Porto, M. A. Soussou, M. Islam, M. Boujtita, K. A. Aissa, L. L. Brizoual, A. Djouadi and T. Brousse, *J. Power Sources*, 2015, **300**, 525-532.

5 R. L. Porto, S. Bouhtiyya, J. F. Pierson, A. Morel, F. Capon, P. Boulet and T. Brousse, *Electrochim. Acta*, 2014, **141**, 203-211.

6 A. Achour, R. L. Porto, M. Chaker, A. Arman, A. Ahmadpourian, M. A. Soussou, M. Boujtita, L. L. Brizoual, M. A. Djouadi and T. Brousse, *Electrochem. Commun.*, 2017, **77**, 40-43.

7 S. Bouhtiyya, R. L. Porto, B. Laïk, P. Boulet, F. Capon, J. P. Pereira-Ramos, T. Brousse and J. F. Pierson, *Scripta. Mater.*, 2013, **68**, 659-662.

8 A. Achour, J. B. Ducros, R. L. Porto, M. Boujtita, E. Gautron, L. L. Brizoual, M. A. Djouadi and T. Brousse, *Nano Energy*, 2014, **7**, 104-113.

9 F. Tian, Y. B. Xie, H. X. Du, Y. Z. Zhou, C. Xia and W. Wang, *Rsc. Adv.*, 2014, **4**, 41856-41863.

10 P. Sun, R. Lin, Z. L. Wang, M. J. Qiu, Z. S. Chai, B. D. Zhang, H. Meng, S. Z. Tan, C. X. Zhao and W. J. Mai, *Nano Energy*, 2017, **31**, 432-440.

11 L. M. Chen, C. Liu and Z. J. Zhang, *Electrochim. Acta*, 2017, **245**, 237-248.

12 Y. J. B. Ting, K. Lian and N. Kherani, *ECS Trans.*, 2011, **35**, 133-139.

13 X. P. Zhou, H. Y. Chen, D. Shu, C. He and J. M. Nan, *J. Phys. Chem. Solids*, 2009, **70**, 495-500.

14 B. Gao, X. Xiao, J. J. Su, X. M. Zhang, X. Peng and J. J. Fu, *Appl. Surf. Sci.*, 2016, **383**, 57-63.

15 S. Z. Wang, L. Zhang, C. L. Sun, Y. L. Shao, Y. Z. Wu, J. X. Lv and X. P. Hao, *Adv. Mater.*, 2016, **28**, 3768-3776.

16 X. H. Lu, G. M. Wang, T. Zhai, M. H. Yu, S. L. Xie, Y. C. Ling, C. L. Liang, Y. X. Tong and Y. Li, *Nano Lett.*, 2012, **12**, 5376-5381.

17 X. Xiao, H. M. Yu, H. Y. Jin, M. H. Wu, Y. S. Fang, J. Y. Sun, Z. M. Hu, T. Q. Li, J. B. Wu, L. Huang, Y. Gogotsi and J. Zhou, *ACS nano*, 2017, **11**, 2180-2186.

18 P. H. Yang, D. L. Chao, C. R. Zhu, X. H. Xia, Y. Q. Zhang, X. L. Wang, P. Sun, B. K. Tay, Z. X. Shen, W. J. Mai and H. J. Fan, *Adv. Sci.*, 2015, **3**, 1500299.

19 Y. B. Xie, Y. Wang and H. X. Du, *Mater. Sci. Eng., B*, 2013, **178**, 1443-1451.

20 C. R. Zhu, P. H. Yang, D. L. Chao, X. L. Wang, X. Zhang, S. Chen, B. K. Tay, H. Huang, H. Zhang, W. J. Mai and H. J. Fan, *Adv. Mater.*, 2015, **27**, 4566-4571.

21 X. H. Lu, M. H. Yu, T. Zhai, G. M. Wang, S. L. Xie, T. Y. Liu, C. L. Liang, Y. X. Tong and Y. Li, *Nano Lett.*, 2013, **13**, 2628-2633.

22 X. Xiao, X. Peng, H. Y. Jin, T. Q. Li, C. C. Zhang, B. Gao, B. Hu, K. F. Huo and J. Zhou, *Adv. Mater.*, 2013, **25**, 5091-5097.